


Article

# PMSM Adaptive Sliding Mode Controller Based on Improved Linear Dead Time Compensation

Huipeng Chen <sup>1</sup>, Zhiqiang Yao <sup>1</sup>, Yongqing Liu <sup>2</sup>, Jian Lin <sup>2</sup>, Peng Wang <sup>2</sup>, Jian Gao <sup>3</sup>, Shaopeng Zhu <sup>3</sup> and Rougang Zhou <sup>1,4,5,\*</sup>

<sup>1</sup> School of Mechanical Engineering, Hangzhou Dianzi University, Hangzhou 310000, China

<sup>2</sup> Mita Group Co., Ltd., Longqian 323700, China

<sup>3</sup> School of Engineering, Zhejiang University, Hangzhou 310058, China

<sup>4</sup> Wenzhou Institute of Hangzhou dianzi University, Wenzhou 325013, China

<sup>5</sup> Mstar Technologies, Inc., Hangzhou 310012, China

\* Correspondence: zhourg@hdu.edu.cn; Tel.: +86-133-4571-6121

**Abstract:** Aiming at the issue of the sliding mode observer (SMO) being sensitive to the motor model parameters at low speeds, a rotor position observation method based on resistance adaptive SMO and considering the influence of inverter dead time is designed in this paper. In this method, the online resistance identification is introduced into the conventional SMO, the resistance parameters of the SMO are modified in real-time, and the online resistance identification algorithm is designed by using the Lyapunov function. An enhanced linear dead time compensation method is proposed to improve the resistance adaptive SMO and eliminate the voltage error between the estimated and the actual motor models in order to address the impact of inverter dead time on the voltage parameters in the estimation model at low speeds. Simulation results show that the online resistance identification and dead time compensation can significantly improve the accuracy of sensorless speed control at low speeds, and the dead time compensation can also improve the accuracy of online resistance identification.

**Keywords:** sliding mode observer; sensorless speed control; low speed; dead time compensation; online resistance identification



**Citation:** Chen, H.; Yao, Z.; Liu, Y.; Lin, J.; Wang, P.; Gao, J.; Zhu, S.; Zhou, R. PMSM Adaptive Sliding Mode Controller Based on Improved Linear Dead Time Compensation. *Actuators* **2022**, *11*, 267. <https://doi.org/10.3390/act11090267>

Academic Editors: Anyang Lu and Ioan Ursu

Received: 1 August 2022

Accepted: 15 September 2022

Published: 19 September 2022

**Publisher's Note:** MDPI stays neutral with regard to jurisdictional claims in published maps and institutional affiliations.



**Copyright:** © 2022 by the authors. Licensee MDPI, Basel, Switzerland. This article is an open access article distributed under the terms and conditions of the Creative Commons Attribution (CC BY) license (<https://creativecommons.org/licenses/by/4.0/>).

## 1. Introduction

A permanent magnet synchronous motor (PMSM) has the advantages of small volume, light weight, simple structure, high efficiency, high torque current ratio, high power density, and low moment of inertia. It has been widely used in the field of industrial drive [1]. As the most reliable and widely used control method in PMSM, vector control needs to obtain the accurate position and speed information of the motor rotor to realize the accurate control of PMSM speed and torque. At present, the common method is to install mechanical sensors (such as the Hall sensor and photoelectric encoder) to obtain position information.

Sensorless speed control is used to maintain the normal operation of the system in the event of hardware sensor failure. There are three main categories of sensorless speed control strategies. The first category is based on the back electromotive force (EMF) method; it estimates the motor speed by observing the back EMF, but the observation result is less accurate at low speeds. The second category relies on high-frequency signal injection, which involves injecting the high-frequency signal and extracting the high-frequency current signal to determine the position information of the motor. Despite torque fluctuation, it has a good observation effect at low and zero speeds. The third category is based on the method of state observer, which not only requires a lot of calculation, but also has an inaccurate estimation effect at low speeds. Except for the second category, sensorless speed control algorithms estimate rotor position information using the PMSM mathematical model. Therefore, the accuracy of the parameters in the PMSM model directly determines

the estimation accuracy of the rotor position, which affects the stability of the whole control system. When there is a high load at low speeds, the resistance voltage drop of stator winding cannot be ignored. At this point, the accuracy of the resistance parameters will play a decisive role in the estimation of the rotor position.

The sliding mode observer (SMO) has been widely used because of its strong robustness, fast dynamic response, and simple engineering implementation [2]. Domestic and foreign experts have proposed several solutions to address the issue of the inaccurate estimation of SMO position information caused by uncertain motor parameters and load torque at low speeds. The adaptive SMO proposed in References [3–7] can simultaneously identify the stator resistance and speed online and eliminate the effect of inaccurate resistance parameters on speed identification at low speeds. On this basis, the super-twisting algorithm (STA) presented in References [8,9] based on the second-order was proposed, which replaces discontinuous functions with an STA. The chattering problem and time delay, which could not be avoided in conventional SMOs, are eliminated in this STA-based second-order SMO. The resistance parameters in SMO designed in Reference [10] are estimated by a fuzzy logic controller (FLC) to achieve a high-performance standard that is simpler and requires less computation. The load torque observed in the SMO in Reference [11] is used as feedforward compensation for the q-axis current, which improves the accuracy of load torque estimation and enhances the SMO's dynamic characteristics and robustness at low speeds. In References [12,13], the disturbance observer (DOB) scheme is used to parallel SMO to estimate the load torque and generate compensation signals to eliminate the load rotation. The transient response of the rotor speed is also improved, reducing the settling time and the maximum overshoot. Reference [14] analyzed the influence of periodic oscillations caused by dead time on the position estimation of SMO rotors and proposed a dead compensation scheme to reduce such position estimation errors. Reference [15] used the recursive restricted total least squares method to estimate voltage distortion amplitude and improve the accuracy of the designed SMO position observation. A new adaptive SMO was proposed in Reference [16]. The back EMF no longer obtained the rotor's position information, but was directly obtained by the stator current, and the stator resistance could be identified simultaneously. Reference [17] proposed an improved SMO. Based on the generalized sliding discrete Fourier transform (GSDFT) strategy, the harmonic components were extracted, the corresponding compensation voltage was calculated, and the intermediate variable H was introduced to expand the back potential at low speeds, which significantly improved the accuracy of low-speed identification. In order to further improve the sensorless control effect of PMSM at low speeds, the SMO based on the back EMF method was studied. The adaptive SMO with online resistance identification was used to estimate the position information of the rotor, and the stability of the system was analyzed according to the Lyapunov stability criterion. The adaptive sliding mode observer was less sensitive to the motor parameters, and could more accurately extract the reaction potential at low speed, and improve the robustness of the controller. At the same time, following low-pass filtering, the high-frequency back EMF signal was angle-compensated according to the speed. On this basis, the influence of inverter nonlinearity on rotor position observation error and online resistance parameter identification was studied, and a better linear dead time compensation method was proposed. When the current was closer to the zero-crossing point, the dead time compensation gain decreased faster, and the gain change rate could be adjusted according to the working environment of the motor. In the case of low speed and light load, the current was very small. The dead zone compensation designed in this paper can effectively avoid the risk of incorrect compensation due to the wrong judgment of current polarity. At the same time, the dead zone compensation gain slope was different, which can fully compensate the current close to zero crossing, and further improve the position observation accuracy and load carrying capacity at low speeds.

In order to demonstrate that the adaptive sliding mode controller and dead time compensation can effectively improve the estimation accuracy of the SMO position infor-

mation at low speeds, it was compared with the conventional SMO by simulation and experiment. The simulation results showed that the accuracy of no speed estimation can be significantly improved by online resistance identification and dead time compensation at low speeds, and the accuracy of online resistance identification can also be improved by dead time compensation.

## 2. Design of Adaptive Sliding Mode Observer

### 2.1. Design of Sliding Mode Observer

The PMSM control belongs to the AC motor control and is a multi-variable, strong coupling, nonlinear, and time-varying complex system. Therefore, for such a complex control system, a mathematical modeling analysis needs to be conducted on it and it needs to be decomposed into a system with controllable variables through mathematical methods. Therefore, the following assumptions are made: (1) the induced electromotive force in the phase winding of the motor is a sine wave; (2) there is no damping winding on the motor rotor; and (3) the core saturation and motor core loss are ignored.

The mathematical model of surface-mounted PMSM ( $L_d = L_q = L$ ) in  $\alpha$ - $\beta$  coordinate can be simplified by ignoring the saturation of the motor iron core, eddy current, hysteresis loss, and other factors [18]:

$$\begin{cases} \frac{di_\alpha}{dt} = -\frac{R_s}{L_s}i_\alpha + \frac{1}{L_s}u_\alpha - \frac{1}{L_s}E_\alpha \\ \frac{di_\beta}{dt} = -\frac{R_s}{L_s}i_\beta + \frac{1}{L_s}u_\beta - \frac{1}{L_s}E_\beta \\ E_\alpha = -\psi_f\omega_e \sin\theta \\ E_\beta = \psi_f\omega_e \cos\theta \end{cases} \quad (1)$$

where  $R_s$  is the stator resistance;  $L_s$  is the stator inductance;  $i_\alpha, i_\beta, u_\alpha, u_\beta$  denote stator currents, the stator voltages of the  $\alpha\beta$  axis;  $E_\alpha$  and  $E_\beta$  are the back EMF of  $\alpha$ - $\beta$  axis;  $\psi_f$  is the permanent magnet flux linkage;  $\omega_e$  is the rotor angular speed; and  $\theta$  is the electrical angle of the rotor.  $i_\alpha, i_\beta, u_\alpha, u_\beta$  denote stator currents, the stator voltages of  $\alpha$ - $\beta$  axis.

The stator current SMO is constructed:

$$\begin{cases} \frac{d\hat{i}_\alpha}{dt} = -\frac{R_s}{L_s}\hat{i}_\alpha + \frac{1}{L_s}u_\alpha - \frac{1}{L_s}Z_\alpha \\ \frac{d\hat{i}_\beta}{dt} = -\frac{R_s}{L_s}\hat{i}_\beta + \frac{1}{L_s}u_\beta - \frac{1}{L_s}Z_\beta \end{cases} \quad (2)$$

where  $\hat{i}_\alpha$  and  $\hat{i}_\beta$  are estimated current.  $Z_\alpha$  and  $Z_\beta$  are control rates:

$$\begin{cases} Z_\alpha = K\text{sign}(i_\alpha - \hat{i}_\alpha) \\ Z_\beta = K\text{sign}(i_\beta - \hat{i}_\beta) \end{cases} \quad (3)$$

where  $K$  is the sliding mode gain coefficient; and  $\text{sign}$  is a switching function.

The sliding surface of the SMO is defined as:

$$S_n = [s_\alpha \quad s_\beta]^T = [\hat{i}_\alpha - i_\alpha \quad \hat{i}_\beta - i_\beta] = [\bar{i}_\alpha \quad \bar{i}_\beta] \quad (4)$$

where  $s_\alpha = \bar{i}_\alpha = \hat{i}_\alpha - i_\alpha$ ,  $s_\beta = \bar{i}_\beta = \hat{i}_\beta - i_\beta$ .

Through Equations (1) and (2), the current deviation equation can be obtained as follows:

$$\begin{cases} \frac{d(\hat{i}_\alpha - i_\alpha)}{dt} = -\frac{R_s}{L_s}(\hat{i}_\alpha - i_\alpha) + \frac{1}{L_s}E_\alpha - \frac{K}{L_s}\text{sign}(\hat{i}_\alpha - i_\alpha) \\ \frac{d(\hat{i}_\beta - i_\beta)}{dt} = -\frac{R_s}{L_s}(\hat{i}_\beta - i_\beta) + \frac{1}{L_s}E_\beta - \frac{K}{L_s}\text{sign}(\hat{i}_\beta - i_\beta) \end{cases} \quad (5)$$

According to the Lyapunov criterion, when the system is stable, the derivative of the energy state equation of the system has the relationship of Equation (5), and based on this, the value of sliding mode gain coefficient is determined, so as to ensure the stability of sliding mode variable structure control system and the accessibility of sliding mode.

The Lyapunov function is constructed as  $V = S(x)^T S(x)/2$ . Then the stability condition of SMO is  $\dot{V} = S(x)^T \dot{S}(x) < 0$ . According to Equation (5), the observer stability condition equation is:

$$\dot{V} = S(x)^T \dot{S}(x) = s_\alpha \dot{s}_\alpha + s_\beta \dot{s}_\beta = \frac{1}{L_s} [(\hat{i}_\alpha - i_\alpha)E_\alpha - K(\hat{i}_\alpha - i_\alpha)\text{sign}(\hat{i}_\alpha - i_\alpha)] + \frac{1}{L_s} [(\hat{i}_\beta - i_\beta)E_\beta - K(\hat{i}_\beta - i_\beta)\text{sign}(\hat{i}_\beta - i_\beta)] - \frac{L_s}{R_s} [(\hat{i}_\alpha - i_\alpha)^2 + (\hat{i}_\beta - i_\beta)^2] \tag{6}$$

According to Equation (6), the value range of sliding mode variable structure gain coefficient under the condition of ensuring system stability:  $K > \max(|E_\alpha|, |E_\beta|)$ .

For a better performance of the adaptive sliding mode controller, a larger  $K$  value must be chosen. However, the larger the  $K$  value is, the larger the chattering of control variables and system state will be. The perturbation upper bounds determine the  $K$  value selection of numerical evaluation. If the perturbation upper bounds are bigger, the corresponding sliding mode gain selection should also be larger in the practical application process. However, it is difficult to select a complex system accurately. There are many disturbances on the upper bound of size, so  $K$  assigns a value through the experience adaptation method.

The low-pass filter can effectively suppress the high-frequency current noise in Equation (3), but it will introduce a certain phase delay, which requires corresponding phase compensation. The compensation angle is shown in Equation (7):

$$\Delta\theta = \tan^{-1}\left(\frac{\omega_e}{\omega_c}\right) \tag{7}$$

### 2.2. Design of Adaptive Sliding Mode Observer

SMO extracts the position information by observing the back EMF of the motor. However, at a low speed, the back EMF is very small, and the voltage drop at the stator is mainly concentrated at the resistance, as shown in Equation (8) below. When the resistance is inaccurate, the rotor position information observed by SMO has a large deviation, which affects the overall control effect of PMSM.

$$\theta = \tan^{-1}\left(\frac{\hat{E}_\alpha}{\hat{E}_\beta}\right) = \tan^{-1}\left(\frac{-\frac{di_\alpha}{dt} - R_s i_\alpha + u_\alpha}{-\frac{di_\beta}{dt} - R_s i_\beta + u_\beta}\right) \tag{8}$$

Therefore, the online resistance parameter identification is introduced, and the identification resistance is fed back to the sliding mode controller in real time to improve the control effect of the sliding mode controller at a low speed.

According to the SMO designed according to Equation (2), the adaptive sliding mode observer with resistance on-line identification is designed as follows [19]:

$$\begin{cases} \frac{d\hat{i}_\alpha}{dt} = -\frac{\hat{R}_s}{L_s}\hat{i}_\alpha + \frac{1}{L_s}u_\alpha - \frac{K}{L_s}\text{sign}(\hat{i}_\alpha - i_\alpha) \\ \frac{d\hat{i}_\beta}{dt} = -\frac{\hat{R}_s}{L_s}\hat{i}_\beta + \frac{1}{L_s}u_\beta - \frac{K}{L_s}\text{sign}(\hat{i}_\beta - i_\beta) \end{cases} \tag{9}$$

where  $\hat{R}_s$  is the estimated stator resistance.

The current deviation equation can be obtained by Equation (1) and Equation (9):

$$\begin{cases} \frac{d(\hat{i}_\alpha - i_\alpha)}{dt} = -\frac{(\hat{R}_s - R_s)}{L_s}\hat{i}_\alpha - \frac{R_s}{L_s}(\hat{i}_\alpha - i_\alpha) + \frac{1}{L_s}E_\alpha - \frac{K}{L_s}\text{sign}(\hat{i}_\alpha - i_\alpha) \\ \frac{d(\hat{i}_\beta - i_\beta)}{dt} = -\frac{(\hat{R}_s - R_s)}{L_s}\hat{i}_\beta - \frac{R_s}{L_s}(\hat{i}_\beta - i_\beta) + \frac{1}{L_s}E_\beta - \frac{K}{L_s}\text{sign}(\hat{i}_\beta - i_\beta) \end{cases} \tag{10}$$

The Lyapunov function is constructed as:

$$V = \frac{1}{2}S(x)^T S(x) + \frac{1}{2}(\hat{R}_s - R_s)^2 \tag{11}$$

The stability condition of SMO is  $\dot{V} = S(x)^T \dot{S}(x) + (\hat{R}_s - R_s)^2 < 0$ . According to Equation (11), the observer stability condition equation is:

$$\dot{V} = [\bar{i}_\alpha \quad \bar{i}_\beta] \begin{bmatrix} -\frac{(\hat{R}_s - R_s)}{L_s} \hat{i}_\alpha - \frac{R_s}{L_s} \bar{i}_\alpha + \frac{1}{L_s} E_\alpha - \frac{K}{L_s} \text{sign} \bar{i}_\alpha \\ -\frac{(\hat{R}_s - R_s)}{L_s} \hat{i}_\beta - \frac{R_s}{L_s} \bar{i}_\beta + \frac{1}{L_s} E_\beta - \frac{K}{L_s} \text{sign} \bar{i}_\beta \end{bmatrix} + (\hat{R}_s - R_s) \dot{\hat{R}}_s < 0 \quad (12)$$

Equation (12) can be disassembled into two equations:

$$[\bar{i}_\alpha \quad \bar{i}_\beta] \begin{bmatrix} -\frac{(\hat{R}_s - R_s)}{L_s} \hat{i}_\alpha \\ -\frac{(\hat{R}_s - R_s)}{L_s} \hat{i}_\beta \end{bmatrix} + (\hat{R}_s - R_s) \dot{\hat{R}}_s = 0 \quad (13)$$

$$[\bar{i}_\alpha \quad \bar{i}_\beta] \begin{bmatrix} -\frac{R_s}{L_s} \bar{i}_\alpha + \frac{1}{L_s} E_\alpha - \frac{K}{L_s} \text{sign} \bar{i}_\alpha \\ -\frac{R_s}{L_s} \bar{i}_\beta + \frac{1}{L_s} E_\beta - \frac{K}{L_s} \text{sign} \bar{i}_\beta \end{bmatrix} < 0 \quad (14)$$

According to Equation (14), the estimated resistance is:

$$\dot{\hat{R}}_s = \frac{1}{L_s} (\bar{i}_\alpha \cdot \hat{i}_\alpha + \bar{i}_\beta \cdot \hat{i}_\beta) \quad (15)$$

From the above, as long as the sliding mode gain  $K > \max(|E_\alpha|, |E_\beta|)$ , it can meet the stability requirements.

The designed adaptive SMO is shown in Figures 1 and 2.

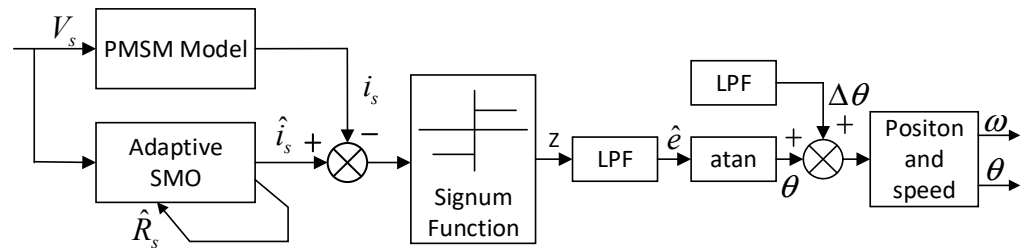


Figure 1. Adaptive SMO.

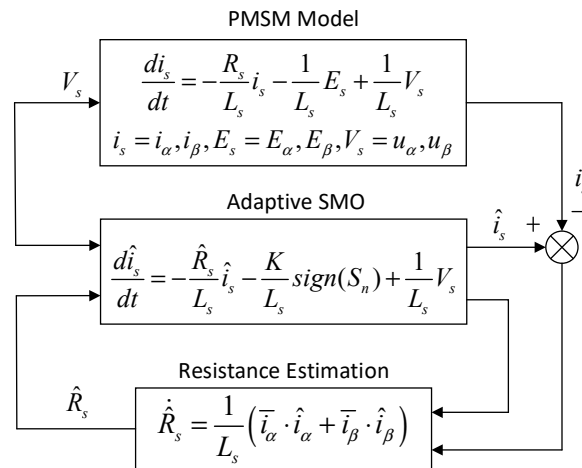


Figure 2. Online resistance parameter identification.

### 3. Analysis and Compensation of the Influence of Dead Time Effect on Observation Error

The turn-on, turn-off times and dead zone settings of the switching device cause nonlinear distortion of the device’s actual output voltage waveform, which results in dead zone effects such as the distorted motor current waveform and torque ripple [20]. The distorted stator current contains fifth and seventh harmonics. After Clark and Park transformation, it contains sixth harmonics in the synchronous rotating coordinate system. Finally, these sixth harmonics will be brought into the  $\alpha$ - $\beta$  axis extended back EMF observed by the SMO, and the SMO’s low-pass filter can filter out the sixth and above harmonics.

However, the SMO cannot filter the voltage distortion which has a significant impact at low speeds.

When PMSM operates stably, the given voltage vector  $U_s$  rotates at the current angular frequency, and the actual voltage space vector  $U_{act}$  is:

$$U_{act} = U_s + \Delta U_i \tag{16}$$

where  $\Delta U_i$  is the error voltage vector. Its size is shown in Figure 3. The amplitude is simply equivalent to  $T_d U_s / T_s$ . Its phase is related to the polarity of the three-phase current. When the polarity of the three-phase currents  $i_a, i_b,$  and  $i_c$  are positive, and positive and negative, the error voltage vector corresponds to  $\Delta U_6$ .

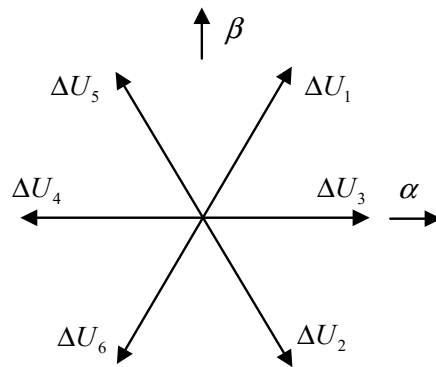


Figure 3. Error voltage vector.

When the polarity of the three-phase currents  $i_a, i_b,$  and  $i_c$  are positive, and positive and negative, the current phase is  $[30^\circ, 90^\circ]$ . It is assumed that the given voltage vector  $U_s$  is ahead of the current vector  $\varphi$ , so the phase of the given voltage vector  $U_s$  is  $[30^\circ + \varphi, 90^\circ + \varphi]$  and the size of the actual voltage vector  $U_{act}$  is shown in Figure 4. In addition,  $\theta$  is the phase of the given voltage vector  $U_s$ ; the included angle between the given voltage vector  $U_s$  and the actual voltage vector  $U_{act}$  is  $\sigma$  and the included angle between the error voltage vector  $\Delta U_6$  and the given voltage vector  $U_s$  is  $\lambda$ .

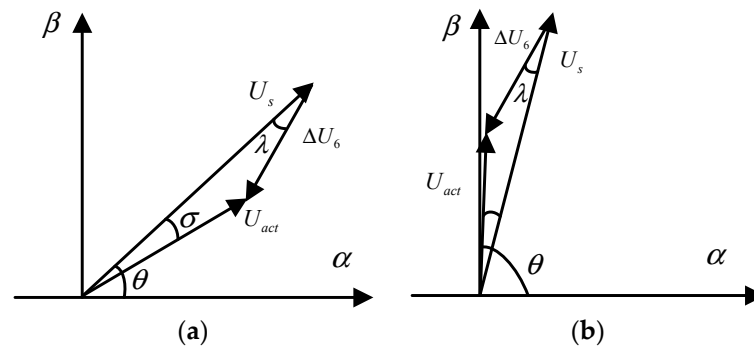


Figure 4. Voltage vector composition diagram when current polarity is positive and negative: (a)  $\theta$  is in  $[30^\circ + \varphi, 60^\circ]$ ; (b)  $\theta$  is in  $[60^\circ, 90^\circ + \varphi]$ .

When  $\theta$  is in  $[30^\circ + \varphi, 60^\circ]$ , the angle  $\lambda$  between error voltage vector  $\Delta U_6$  and voltage vector  $U_s$  is:

$$\lambda = 60^\circ - \theta \tag{17}$$

Therefore, the amplitude of the actual voltage vector  $U_{act}$  can be obtained:

$$|U_{act}| = \sqrt{|U_s|^2 + |\Delta U_6|^2 - 2|U_s| \cdot |\Delta U_6| \cdot \cos \lambda} \tag{18}$$

The phase of the actual voltage vector  $U_{act}$  lagging behind the given voltage vector  $U_s$  is:

$$\sigma = \arcsin(|\Delta U_6| \cdot \sin \lambda / |U_{act}|) \tag{19}$$

Then it can be concluded that the phase of the actual voltage vector  $U_{act}$  is:

$$\theta_{act} = \theta - \sigma \tag{20}$$

Similarly, when  $\theta$  is in  $[60^\circ, 90^\circ + \varphi]$ :

$$\lambda = \theta - 60^\circ \tag{21}$$

At this time, the actual voltage vector  $U_{act}$  is ahead of the given voltage vector  $U_s$ , and the phase is:

$$\theta_{act} = \theta + \sigma \tag{22}$$

The actual voltage vectors of the other five current polarity sectors can be inferred according to the same theory. Assuming the dead time  $T_d = 7 \mu s$ , the bus voltage  $U_{dc} = 310 \text{ V}$ , and the PWM switching time  $T_s = 100 \mu s$ , the error voltage amplitude can be obtained as 21.7 V. Additionally, the results shown in Figure 5 can be obtained assuming that the given voltage vector is ahead of the current vector and has an amplitude.

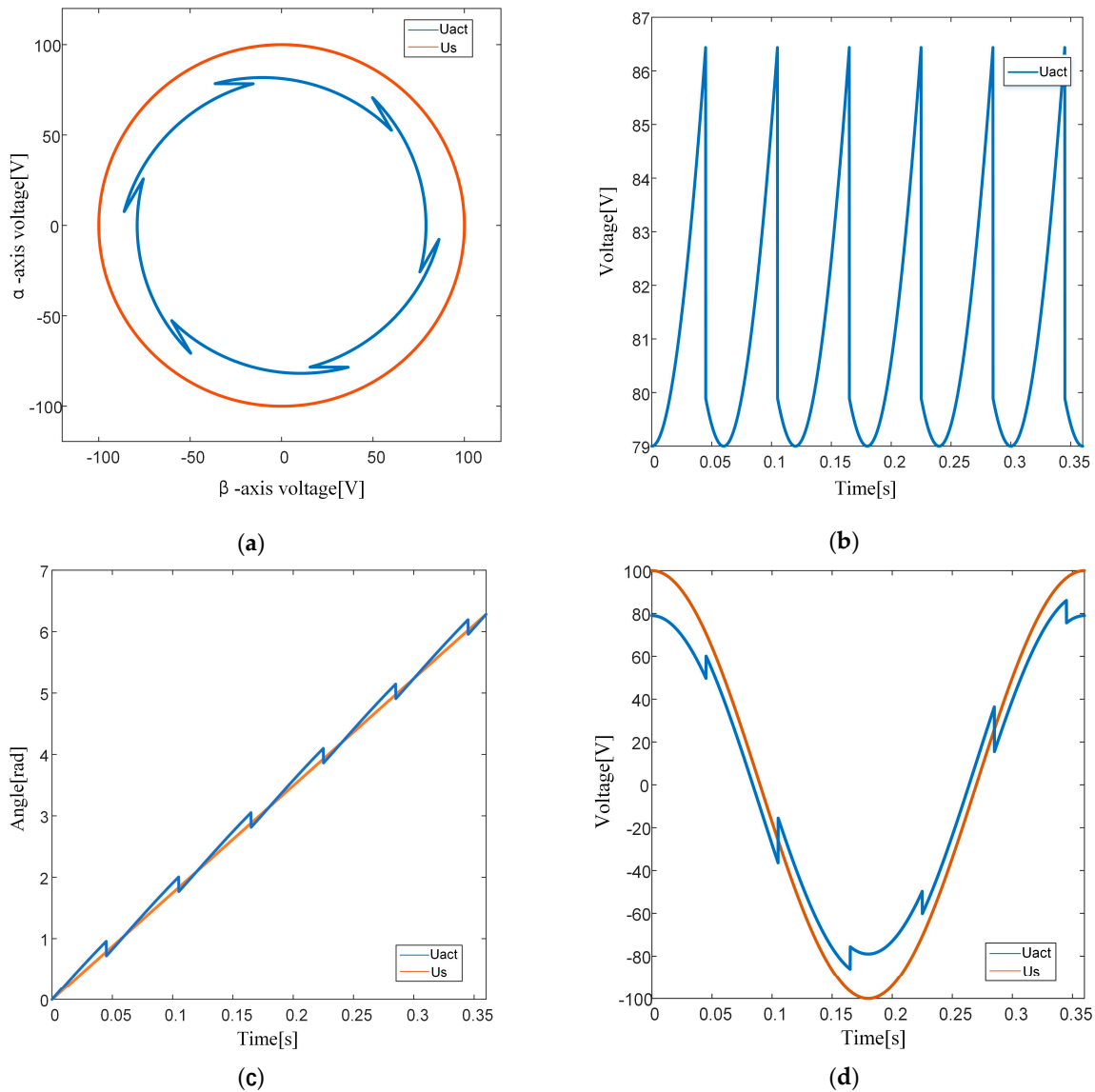


**Figure 5.** Waveform of dead time effect: (a) The ideal voltage and the actual voltage between  $\alpha$  axis and  $\beta$  axis; (b) actual voltage amplitude; (c) the phase between the actual voltage and the ideal voltage; (d) actual phase voltage and ideal phase voltage.

According to the aforementioned results, there is a large deviation between the actual and the given voltages due to the existence of a dead zone, and the adaptive SMO uses the given voltage to determine the speed and the resistance. Therefore, it is necessary to introduce dead time compensation to reduce this deviation and improve the adaptive SMO’s observation effect at low speeds.

Accurate three-phase current polarity determination is the key technical component of dead time compensation. The three-phase current contains more harmonics, particularly at low speeds, so it is impossible to directly determine its polarity. Therefore, this paper processes the DC component on the synchronous rotation coordinate to identify the current polarity. First, the DC component is low-pass filtered (the interference signal is removed and there is no phase lag), then the ipark transform is carried out (the  $\alpha$ - $\beta$  axis current is obtained), and the arctangent of the current is finally used to calculate the current phase. The current polarity is then determined accordingly. The corresponding three-phase dead time compensation voltages  $U_{a1}$ ,  $U_{b1}$  and  $U_{c1}$  can be obtained through the current polarity. The compensation scheme is shown in Figure 6.

$$[U_{a1} \ U_{b1} \ U_{c1}]^T = \Delta U_i [f(i_a) \ f(i_b) \ f(i_c)]^T \tag{23}$$

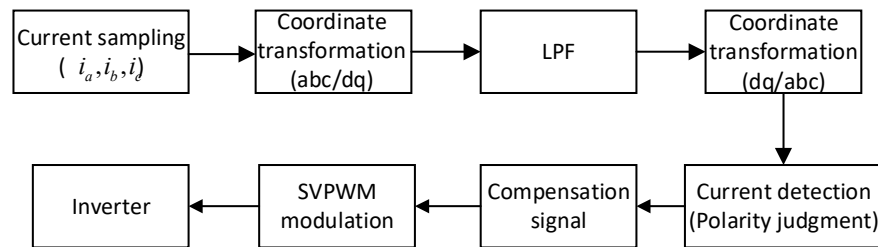


Figure 6. Dead zone compensation.

When the current crosses the zero point, it is difficult to determine the current polarity. If the identified polarity is incorrect, it will even aggravate the dead time effect, particularly at low speeds and low voltages. Therefore, this paper used the improved linear compensation method to compensate for the dead time, as the compensation gain is in the form of a quadratic function near the current zero-crossing. The principle is shown in Figure 7. The size of  $m$  is affected by hardware conditions, and 4% of the rated current was taken in this paper. When the current is less than  $m$ , the compensation gain decreases as the current approaches the zero-crossing point, which can effectively avoid the risk of false compensation due to the incorrect identification of current polarity.

$$f(i) = \begin{cases} \text{sign}(i) \cdot \left(\frac{i}{m}\right)^2 & |i| < m \\ \text{sign}(i) & |i| \geq m \end{cases} \tag{24}$$

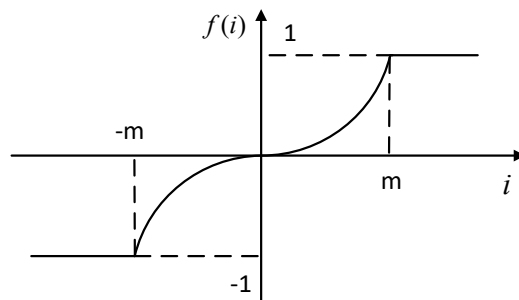


Figure 7. Improved linear compensation function.

#### 4. Analysis of Simulation Results

The principal block diagram of the adaptive sliding mode observer algorithm based on the improved linear dead time compensation proposed in this paper is shown in Figure 8.



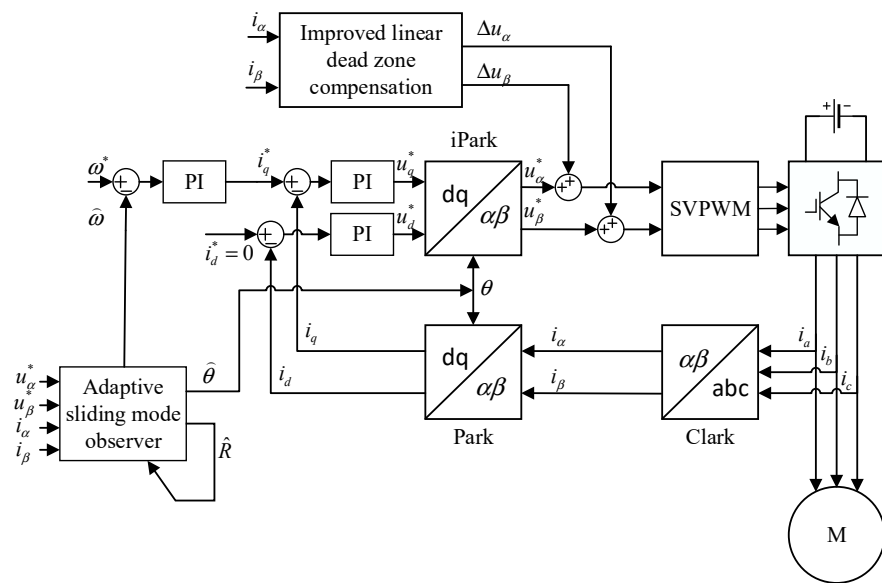


Figure 8. Block diagram of algorithm principle.

In order to verify the improved effect, the simulation verification is carried out in Matlab/Simulink, and the selected motor parameters are shown in Table 1.

Table 1. Parameters of simulated motor.

Parameter	Value
Rated line voltage/V	310
Rated line current/A	3
Rated power/W	750
Rated speed/(r/min)	2500
Stator phase resistance/ $\Omega$	1.68
Inductance/mH	3.2
Permanent magnet fluxlinkage/Wb	0.093
Polar	4

Figures 9–12 are the simulation waveforms of the traditional sliding mode observer and the adaptive sliding mode observer based on improved linear dead time compensation under the control of  $i_d = 0$ . The simulation time is 0.4 s, the simulation step is 0.001 s, the given speed is 300 r/min, and the load torque of  $2.5 \text{ N} \cdot \text{m}$  is suddenly added at 0.2 s.

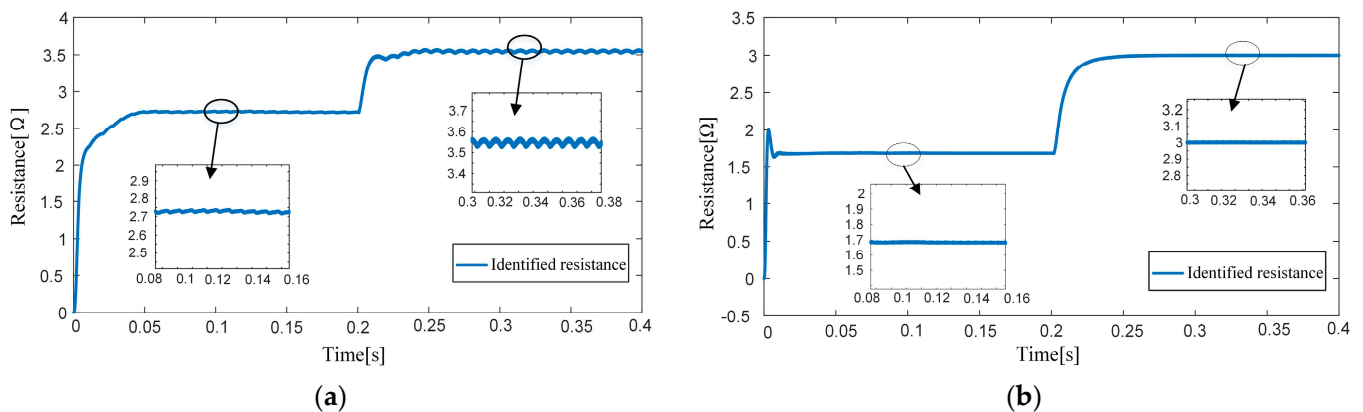
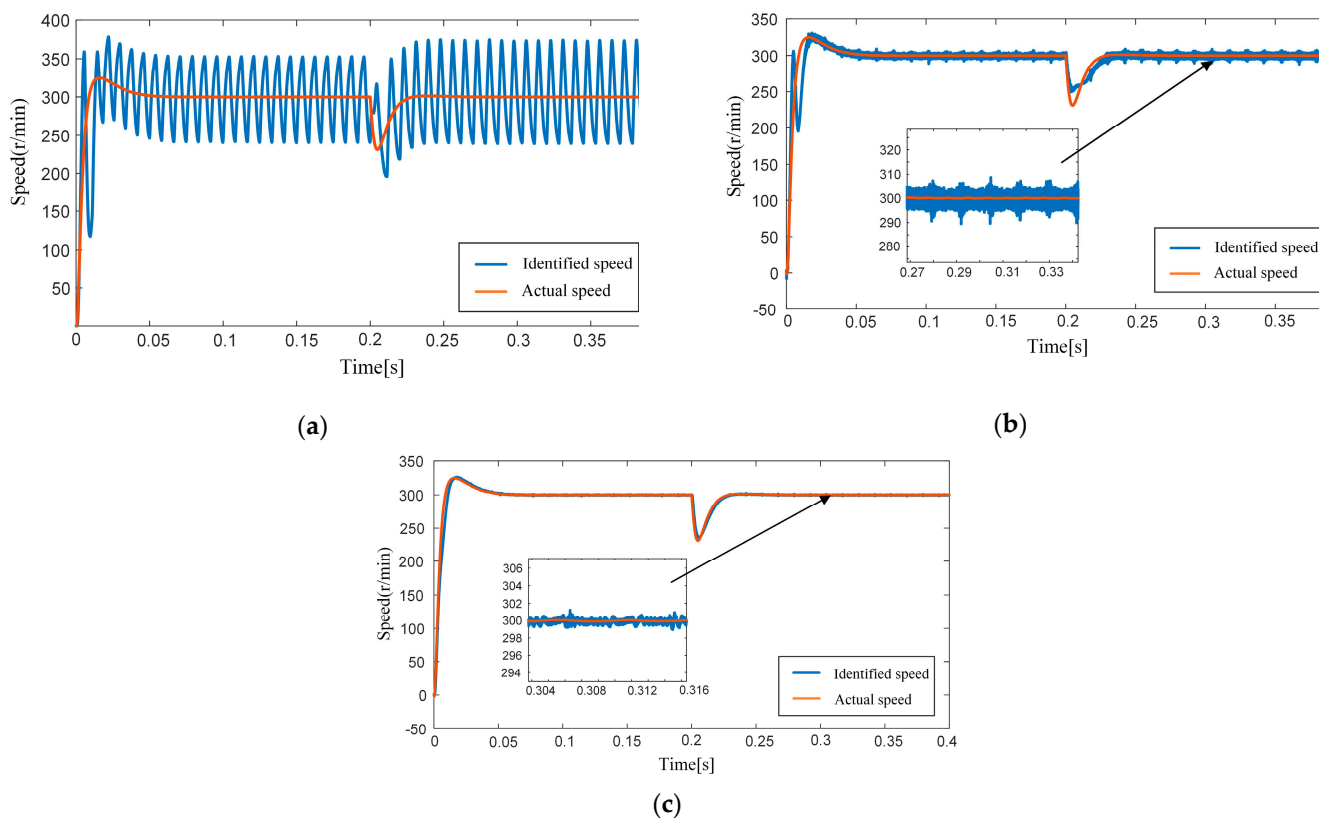
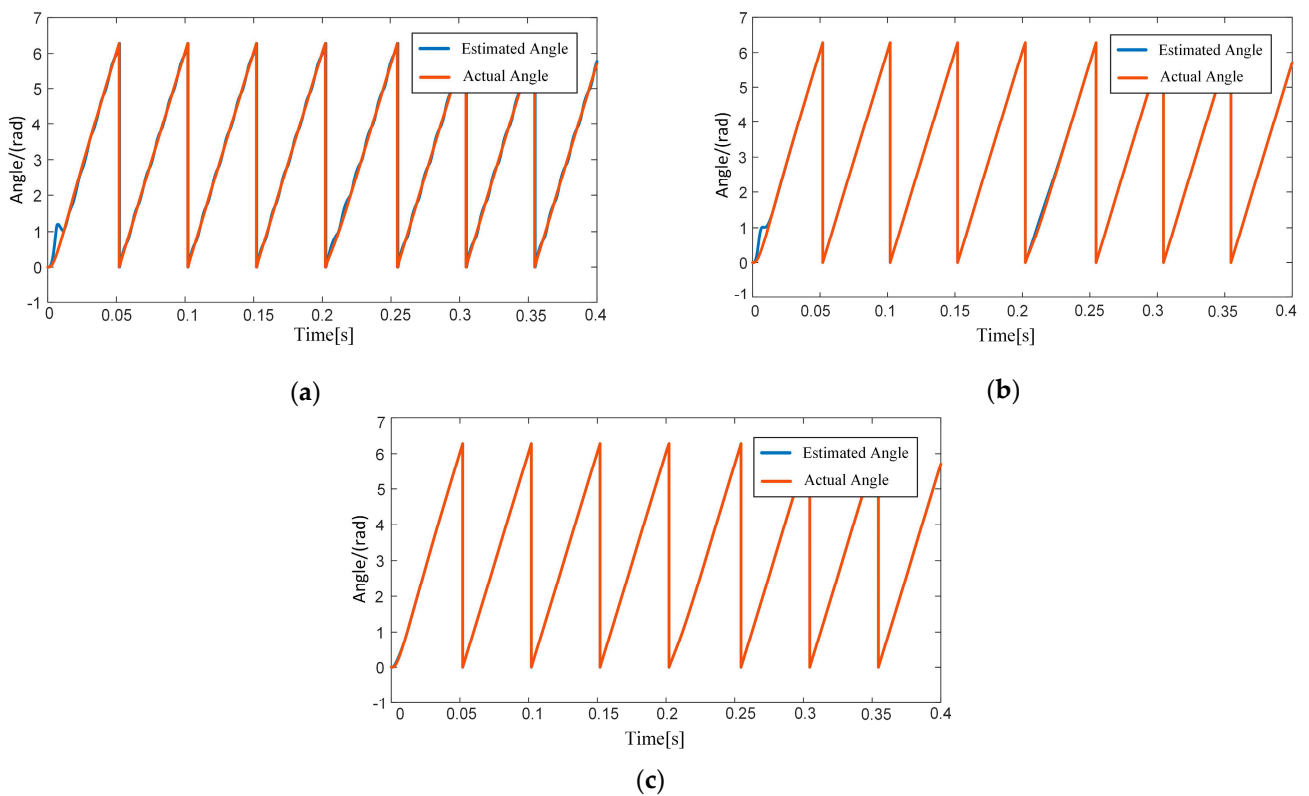


Figure 9. Resistance identification waveform: (a) Adaptive sliding mode observer; (b) adaptive sliding mode observer + dead zone compensation.



**Figure 10.** Speed estimation waveform: (a) The traditional sliding mode; (b) the traditional sliding mode + dead zone compensation; (c) adaptive sliding mode observer + dead zone compensation.



**Figure 11.** Angle estimation waveform: (a) The traditional sliding mode; (b) the traditional sliding mode + dead zone compensation; (c) adaptive sliding mode observer + dead zone compensation.

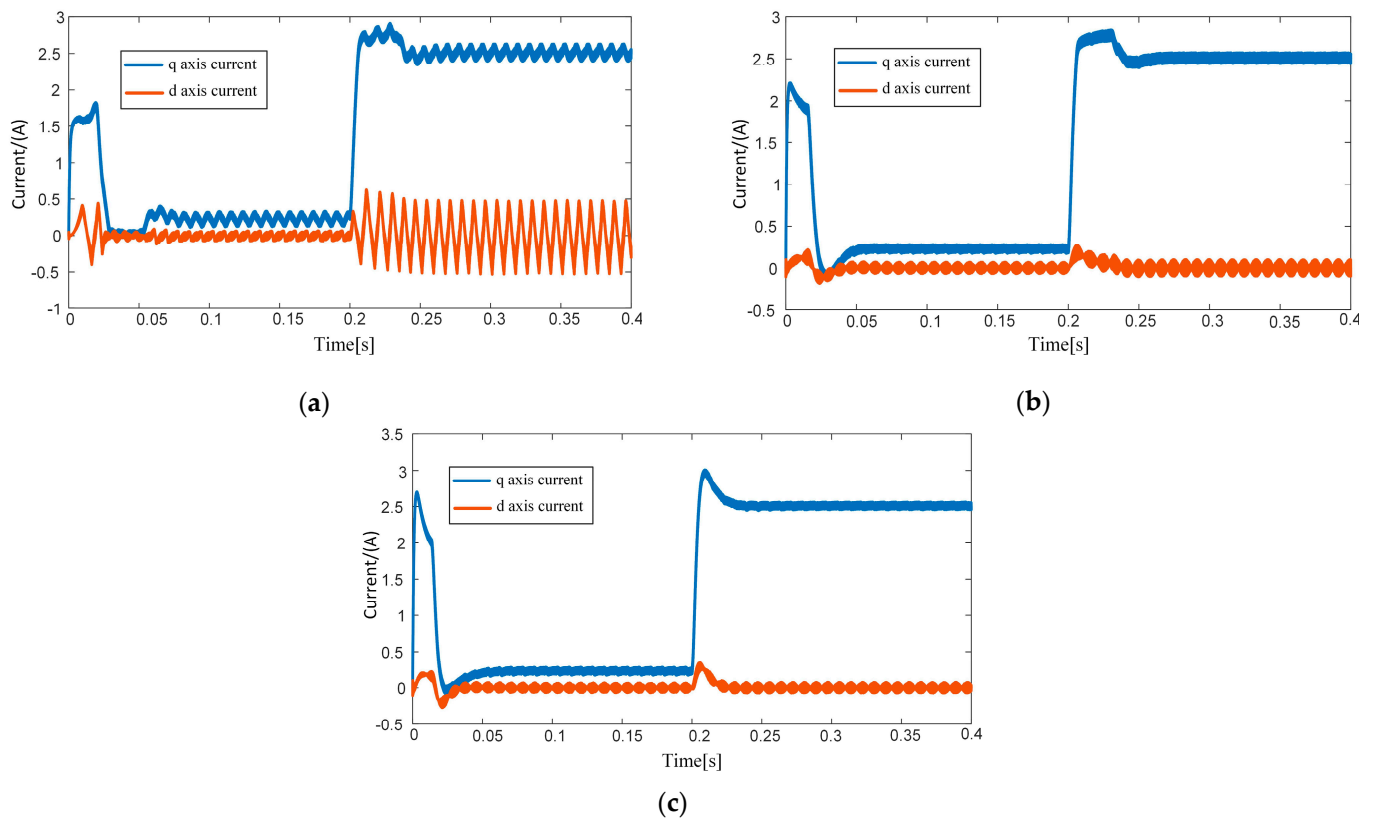


**Figure 12.** d-q axis current waveform: (a) The traditional sliding mode; (b) the traditional sliding mode + dead zone compensation; (c) adaptive sliding mode observer + dead zone compensation.

Figure 9 shows the resistance identification of the adaptive SMO under a 7  $\mu$ s dead time, both before and after the improved linear dead time compensation. The motor resistance is changed from 1.68 to 3  $\Omega$  at 0.2 s. It can be seen from Figure 9a that there is a large error in resistance identification without dead zone compensation. After introducing dead zone compensation in Figure 9b, the resistance identification error is within 0.05  $\Omega$ , which demonstrates that the dead zone has a significant impact on the accuracy of resistance identification. At the same time, the improvement of linear dead zone compensation can significantly improve the accuracy of online resistance identification. In [21], the second-order sliding mode observer (STA-SMO) with the supertorsion algorithm is used to estimate the stator resistance ( $R_s$ ) and rotor position information online, in order to consider the influence of the dead zone. In this paper, the dead zone effect was considered and the improved nonlinear dead zone compensation was adopted. In [21], the resistance of the motor is 2.785  $\Omega$ , and the resistance error identified by STA-SMO is about 0.2  $\Omega$ . According to the above results, the resistance identification accuracy of the observer designed in this paper is higher than that in [21].

Figures 10–12 show the observed waveforms of speed, electrical angle, and the d-q axis current, respectively, observed by both the improved adaptive SMO and the conventional one, under the condition of low speed (300 r/min). The actual phase resistance of the motor is 1.68, the given resistance of the SMO is 3  $\Omega$ , and the dead time is 7  $\mu$ s. It can be seen from Figure 10a that the speed observation of the conventional SMO has a deviation of 50 r/min, and the observation effect is very poor. Figure 10b demonstrates that after improved linear dead time compensation, the speed observation error of the conventional SMO is less than 10 r/min, which has an obvious improvement effect. On this basis, the resistance is identified online in Figure 10c. The speed deviation can be controlled within 2 r/min, and the speed observation effect can be further improved. When the motor is 500 r/min, the observed electrical angle of STA-SMO designed in [21] has a certain deviation, and the observed speed has a deviation of 5–10 r/min. When the rotor is 300 r/min, the electric

angle of the observer designed in this paper has no deviation, and the speed is controlled within 2 r/min. The observer designed in this paper has better performance.

It can be seen from Figure 11 that the conventional SMO has a significant deviation in the estimation of the electrical angle during startup and sudden load change. After improved linear dead time compensation and resistance identification, the observed and the actual electrical angles are basically consistent, and the improvement effect is obvious. Figure 12 shows that under the conventional sliding mode control, the d-q axis current fluctuates significantly, the torque waveform is large, and the overall control effect of the motor is poor. Following the improved linear dead time compensation, the d-q axis current fluctuation is significantly improved. At the same time, after the introduction of online resistance identification, the d-q axis current essentially has no fluctuation.

The simulation diagram of phase current and spectrum before and after dead time compensation is shown in Figures 13 and 14. The dead time in motor is 7  $\mu$ s. Through comparative analysis, it can be seen that at a low speed and low load, the sinusoidal degree of the phase current waveform without dead time compensation is very large, the zero current clamp phenomenon is obvious, and there are more fifth and seventh harmonics, and there is serious phase current distortion. After the traditional linear dead zone compensation, the sinusoidal degree is improved, and the fifth and seventh harmonics are also reduced, but the effect is not very good. The improved linear dead time compensation proposed in this paper can significantly improve the sinusoidal degree of phase current, eliminate the zero-clamp region phenomenon, reduce the amplitude of the fifth and seventh harmonics, and eliminate the distortion phenomenon. Compared with the traditional linear dead zone compensation, it has a significant improvement.

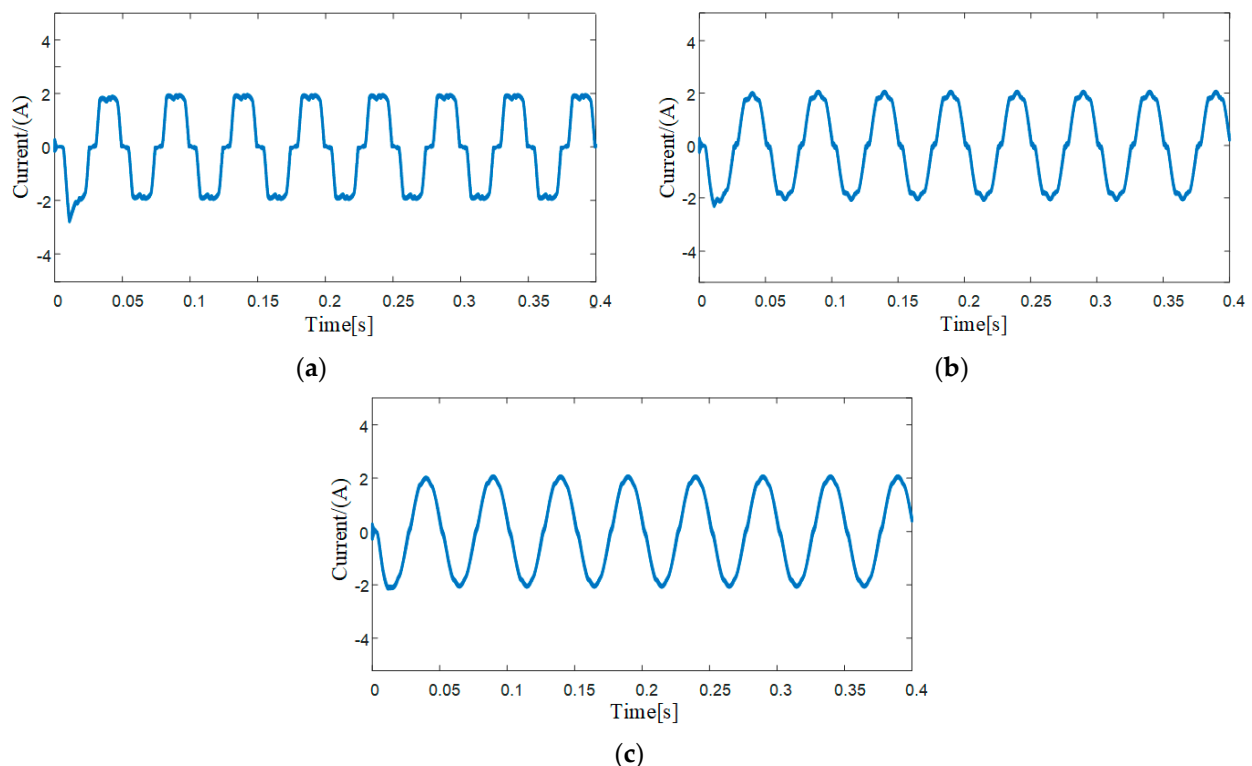


**Figure 13.** Phase current waveform: (a) No dead zone compensation; (b) the traditional linear dead zone compensation; (c) the improved linear dead time compensation.

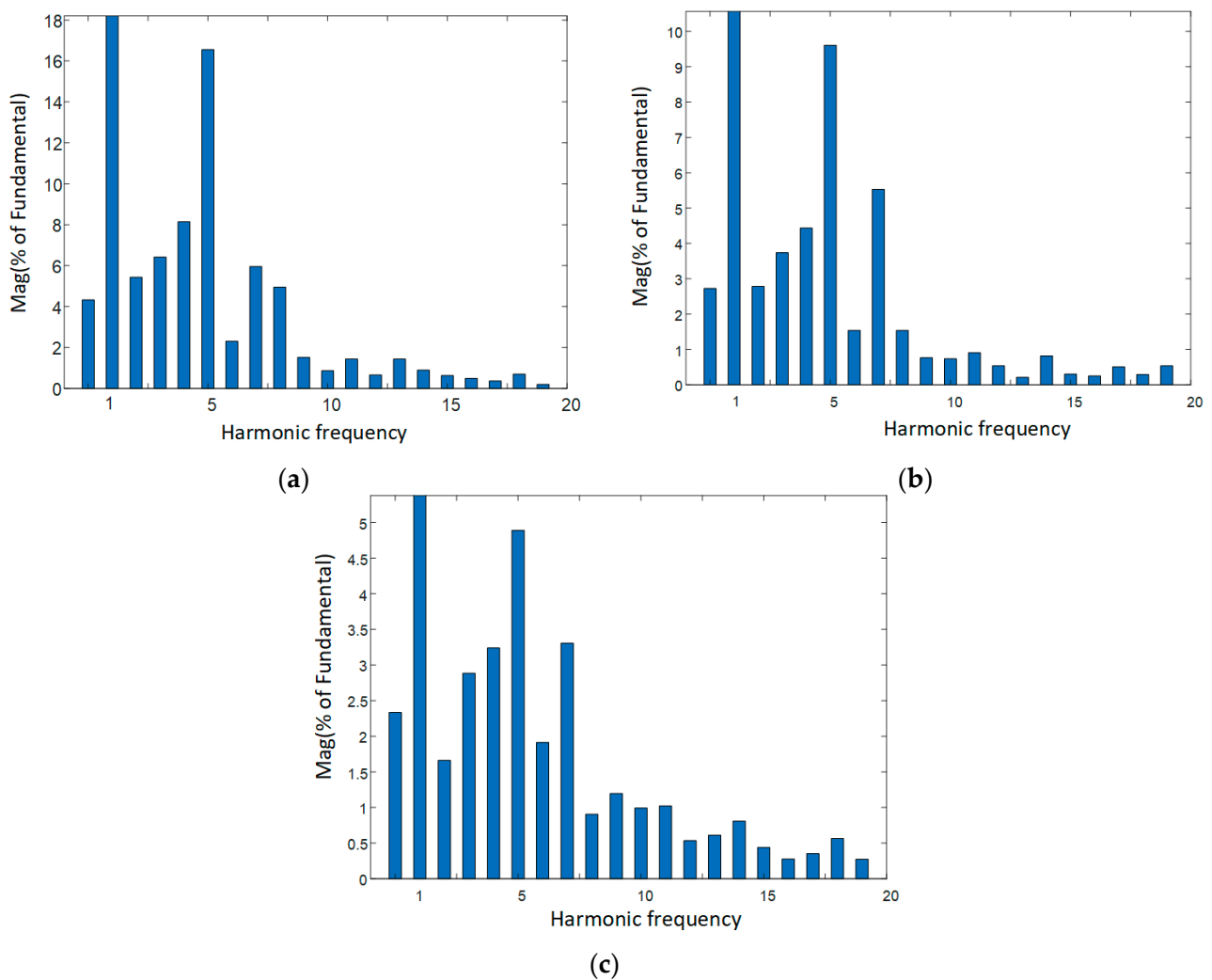


**Figure 14.** Fast Fourier transform (FFT) waveform: (a) No dead zone compensation; (b) the traditional linear dead zone compensation; (c) the improved linear dead time compensation.

Simulation results show that the dead time effect and inaccurate resistance parameters of the SMO have a significant impact on the estimation of rotor position information at low speeds. The enhanced linear dead time compensation and adaptive sliding mode controller proposed in this paper can improve the dead time effect and accurately identify the resistance parameters under the condition of stable convergence of the algorithm. Upon an abrupt change in the load torque, the position information can also be observed accurately, and the current overshoot is small, which significantly improves the position observation accuracy and robustness of the SMO at low speeds.

## 5. Conclusions

Aiming at the SMO's sensitivity to resistance parameters and the influence of the dead time effect at low speeds, an adaptive SMO is proposed to observe the rotor position information based on improved linear dead time compensation. In this scheme, the resistance parameters are identified online, the parameters of the SMO are modified by real-time feedback, and the improved linear dead time compensation is introduced. The latter improves not only the position effect of the SMO, but also the accuracy of the online resistance identification. The accuracy of the parameters in the motor model used by the algorithm is guaranteed, and the sensitivity of the SMO to these parameters at low speeds is reduced. Simulation results demonstrate that this scheme can accurately estimate the rotor position information at low speeds and abrupt loads and improve the robustness

to motor parameters. Since it is a simulation experiment, the controller involved in this paper is not very convincing, so experimental verification will be carried out in future experiments. At the same time, the meta-heuristic learning algorithm is very popular in the current application because it can determine the optimal solution within the desired range of the controller and has a low computational cost and high optimization efficiency. In future studies, the meta-heuristic algorithm will be combined to estimate the electronic parameters and torque ripple to improve the controller's stability further. However, since the proposed method is based on the fundamental model, it cannot operate at zero or ultra-low speeds. Therefore, the high-frequency injection algorithm is adopted to realize the stable control of the full-speed section of the controller.

**Author Contributions:** Conceptualization, methodology, H.C.; investigation, formal analysis, Z.Y. and Y.L.; validation, writing—original draft preparation, J.L. and P.W.; supervision, writing—review and editing, J.G. and S.Z.; funding acquisition, R.Z. All authors have read and agreed to the published version of the manuscript.

**Funding:** We gratefully acknowledge the financial support of this research by the following projects: Control design of new energy vehicle air conditioning compressor based on intelligent multi-objective optimization (Grant No. ZDLQ2020002), Research on the theory and method of autonomous cooperative operation control of high-speed trains (Grant No. U1934221) and Research and manufacture of high precision grinding process of wear-resistant seals of construction machinery (Grant No. ZDLQ2021005).

**Data Availability Statement:** Not applicable.

**Conflicts of Interest:** The authors declare no conflict of interest.

## References

1. Maiti, S.; Chakraborty, C. Model Reference Adaptive Controller-Based Rotor Resistance and Speed Estimation Techniques for Vector Controlled Induction Motor Drive Utilizing Reactive Power. *IEEE Trans. Ind. Electron.* **2008**, *55*, 594–601. [\[CrossRef\]](#)
2. Cheng, X.; Liu, H.; Lu, W. Chattering-Suppressed Sliding Mode Control for Flexible-Joint Robot Manipulators. *Actuators* **2021**, *10*, 288. [\[CrossRef\]](#)
3. Wibowo, W.K.; Jeong, S.K. Improved estimation of rotor position for sensorless control of a PMSM based on a sliding mode observer. *J. Cent. South Univ.* **2016**, *23*, 1643–1656. [\[CrossRef\]](#)
4. Hosseyni, A.; Trabelsi, R.; Iqbal, A. An improved sensorless sliding mode control/adaptive observer of a five-phase permanent magnet synchronous motor drive. *Int. J. Adv. Manuf. Technol.* **2017**, *93*, 1029–1039. [\[CrossRef\]](#)
5. Iliudis, V.C.; Margaris, N.I. Sensorless Sliding Mode Observer based on rotor position error for salient-pole PMSM. In Proceedings of the Mediterranean Conference on Control and Automation, Thessaloniki, Greece, 24–26 June 2009.
6. Han, Y.-S.; Choi, J.-S.; Kim, Y.-S. Sensorless PMSM drive with a sliding mode control based adaptive speed and stator resistance estimator. *IEEE Trans. Ind. Magnetics.* **2000**, *36*, 3588–3591. [\[CrossRef\]](#)
7. Han, Y.S.; Kim, Y.S. Sensorless control of Permanent Magnet Synchronous Motor based on rotating coordinate system considering dead-time. In Proceedings of the IEEE International Conference on Power and Power and Renewable Energy (ICPRE), Shanghai, China, 21–23 October 2016.
8. Liang, D.; Li, J.; Qu, R. Sensorless Control of Permanent Magnet Synchronous Machine Based on Second-Order Sliding-Mode Observer With Online Resistance Estimation. *IEEE Trans. Ind. Appl.* **2017**, *53*, 3672–3682. [\[CrossRef\]](#)
9. Liang, D.; Li, J.; Qu, R. Super-twisting algorithm based sliding-mode observer with online parameter estimation for sensorless control of permanent magnet synchronous machine. In Proceedings of the IEEE Energy Conversion Congress and Exposition, Milwaukee, WI, USA, 18–22 September 2016.
10. Habbi, H.M.D.; Surong, H. Sensorless Control Approach Based Adaptive Fuzzy Logic Controller for IPMSM Drive with an On-line Stator Resistance Estimation. In Proceedings of the Pacific-Asia Conference on Knowledge Engineering and Software Engineering, Shenzhen, China, 19–20 December 2009.
11. Lu, W.; Zheng, D.; Lu, Y. New Sensorless Vector Control System with High Load Capacity Based on Improved SMO and Improved FOC. *IEEE Access.* **2021**, *9*, 40716–40727. [\[CrossRef\]](#)
12. Lee, K.; Choy, I.; Back, J. Disturbance observer based sensorless speed controller for PMSM with improved robustness against load torque variation. In Proceedings of the 8th International Conference on Power Electronics, Jeju, Korea, 30 May–3 June 2011.
13. Apte, A.; Joshi, V.A.; Mehta, H.; Walambe, R. Disturbance-Observer-Based Sensorless Control of PMSM Using Integral State Feedback Controller. *IEEE Trans. Ind. Electron.* **2019**, *35*, 6082–6090. [\[CrossRef\]](#)
14. Zhao, Y.; Qiao, W.; Wu, L. Dead-Time Effect Analysis and Compensation for a Sliding-Mode Position Observer-Based Sensorless IPMSM Control System. *IEEE Trans. Ind. Appl.* **2014**, *51*, 2528–2535. [\[CrossRef\]](#)

15. Wang, Y.; Xu, Y.; Zou, J. Sliding-Mode Sensorless Control of PMSM with Inverter Nonlinearity Compensation. *IEEE Trans. Ind. Electron.* **2019**, *34*, 10206–10220. [[CrossRef](#)]
16. Wesub, E.; Imyong, K.; Jang, L. Enhancement of the speed response of PMSM sensorless control using an improved adaptive sliding mode observer. *Ind. Electron.* **2008**, 188–192.
17. Yuan, Q.; Yang, Y.; Wu, H. Low Speed Sensorless Control Based on an Improved Sliding Mode Observation and the Inverter Nonlinearity Compensation for SPMSM. *IEEE Access.* **2020**, *8*, 61299–61310. [[CrossRef](#)]
18. Kim, H.; Son, J.; Lee, J. A High-Speed Sliding-Mode Observer for the Sensorless Speed Control of a PMSM. *IEEE Trans. Ind. Electron.* **2011**, *58*, 4069–4077.
19. Zhou, C.; Zhou, Z.; Tang, W.; Yu, Z. Improved Sliding-Mode Observer for Position Sensorless Control of PMSM. In Proceedings of the 2018 Chinese Automation Congress (CAC), Xi'an, China, 30 November–2 December 2018.
20. Ben-Brahim, L. On the compensation of dead time and zero-current crossing for a PWM-inverter-controlled AC servo drive. *IEEE Trans. Ind. Electron.* **2004**, *51*, 1113–1118. [[CrossRef](#)]
21. Wang, T.; Hu, G.; Yu, Q. An Improved Sensorless Control Scheme for PMSM with Online Parameter Estimation. In Proceedings of the 2021 IEEE 16th Conference on Industrial Electronics and Applications (ICIEA), Chengdu, China, 1–4 August 2021.